



Material properties

On the difference in material structure and fatigue properties of nylon specimens produced by injection molding and selective laser sintering



Brecht Van Hooreweder^{a,*}, David Moens^{a,b}, Rene Boonen^a, Jean-Pierre Kruth^a, Paul Sas^a

^a KU Leuven, Department of Mechanical Engineering, PMA, Celestijnenlaan 300b, 3001 Leuven, Belgium

^b Thomas More Mechelen, Campus De Nayer, J. De Nayerlaan 5, 2860 Sint-Katelijne-Waver, Belgium

ARTICLE INFO

Article history:

Received 19 March 2013

Accepted 30 April 2013

Keywords:

Selective laser sintering

Injection molding

Polyamide 12

Microstructure

Fatigue behavior

ABSTRACT

This paper describes the influence of dynamic tension/compression loading on notched and unnotched nylon specimens fabricated by Injection Molding (IM) and Selective Laser Sintering (SLS). The main objective of this work is to analyze and describe the differences in material structure and fatigue properties of as-built nylon parts produced by IM and SLM from the same polyamide 12 powder. The differences in dimensional quality, density, surface roughness, crystal structure and crystallinity are systematically measured and linked to the mechanical fatigue properties. The fatigue properties of the unnotched SLS specimens are found to be equal to those of the unnotched IM specimens. The presence of pores in the sintered samples does not lead to rapid failure, and the microvoid coalescence failure mechanism is delayed. The notched specimens show more brittle failure and increased fatigue resistance which is caused by local notch-strengthening. The results enable improved understanding of the difference in material structure and fatigue behavior of selective laser sintered and injection molded polyamide.

© 2013 Elsevier Ltd. All rights reserved.

1. Introduction

Selective laser sintering (SLS) is an additive manufacturing process in which layers of preheated powder are spread and laser radiation is used to liquefy (either partially or fully) and fuse the powdered material [1]. Sintered material forms parts, whilst un-sintered material remains in place to support the structure. The build platform is slowly cooled to room temperature after sintering to avoid shrinkage and distortion of the final products. Selective laser sintering has evolved from a rapid prototyping (RP) technique to a promising additive manufacturing (AM)

technique. Sintered parts in polyamide are increasingly being used for functional applications in the automotive, aerospace and biomedical industries [2,3]. The SLS process offers a number of advantages over conventional production techniques, such as injection molding (IM): short design to manufacturing cycle time, high geometrical freedom, customized components and inexpensive production of small numbers of parts. However, to be competitive with the conventional production techniques, the mechanical properties of the SLS components must be sufficient to meet in-service loading and operational requirements.

A number of studies have been performed to optimize the mechanical properties using polymer blends [4–8]. Also, the influence of various process parameters such as energy density, cooling rate, scan pattern, layer orientation, delay time, etc. has been analyzed to find an optimal set of production parameters [9–13]. Although the mechanical

* Corresponding author. Tel.: +32 16 328607; fax: +32 16 322838.

E-mail address: brecht.vanhooreweder@mech.kuleuven.be (B. Van Hooreweder).

properties of sintered material are of significant importance, very little has been reported in literature on the fatigue properties of sintered polyamide components. Knowledge of the fatigue properties of these sintered materials is limited and accurate fatigue life predictions are, therefore, not possible.

In a previous study, the authors made a first attempt to address this by studying the fatigue failure of unnotched SLS-PA12 components under tension/compression loading [14]. In the present work, notched and unnotched SLS specimens are subjected to the same fatigue loading and compared with notched and unnotched IM specimens. All the specimens were produced from the same powder particles and the quality of the end-products was carefully examined prior to fatigue testing. Consequently, a true comparison between IM and SLS specimens is made.

Fig. 1 shows an overview of the most important parameters influencing the fatigue life of PA12 components produced by selective laser sintering or injection molding. The fatigue life depends on the fatigue testing conditions and the properties of the final parts. These final part properties are functions of the powder quality and process parameters. This work presents a systematic description of process parameters, powder quality and final part properties which is then linked to the experimentally determined mechanical fatigue behavior.

2. Test specimens

2.1. Material and geometry

It is well known that powder properties and dimensions are important for the quality of laser sintered parts. To

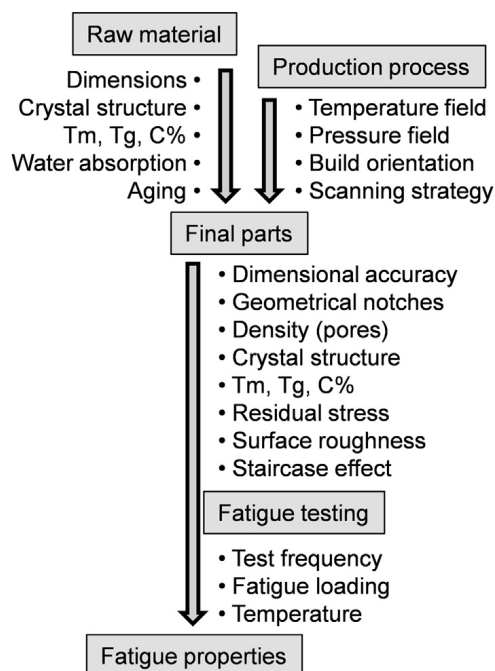


Fig. 1. Overview of parameters influencing the fatigue life of SLS and IM components.

minimize the influence of the raw material on the mechanical properties of the specimens, one unique batch of semi-crystalline polyamide 12 (PA12) powder was used for the production of the specimens with both SLS and IM. Fig. 2 shows a scanning microscope observation of these powder particles indicating the semi-spherical geometry with average diameter of 60 μm .

Fig. 3 shows the geometry of the notched and unnotched cylindrical specimens that were used for the fatigue experiments. The geometry of the test specimens was chosen according to ISO1352 (rotating bar bending fatigue testing) so that the parts could be subjected to fluctuating bending and torsion stresses in a multi-axial fatigue test rig designed at KU Leuven [15]. Using finite element analysis, the geometrical stress concentration factors were calculated to be 1.02 for the unnotched geometry and 2.12 for the notched geometry.

2.2. Selective laser sintering

Selective laser sintering was used to produce 80 cylindrical test specimens from semi-crystalline polyamide 12 powder. To study the influence of the scanning direction on the mechanical properties, two different orientations were produced. Both the notched and unnotched specimen geometries were manufactured with longitudinal axis along the scan-direction (x) and with longitudinal axis perpendicular to the scan direction (x), as indicated in Fig. 4. In the first case (A), parts are built up layer by layer along the z-direction, and the scan direction corresponds with the loading direction. In the second case (B), parts are also built up in the z-direction but the scan direction is perpendicular to the loading direction.

Table 1 shows the SLM process parameters used in a previous study by Van Hooreweder and also used in this work [14]. With these parameters, high quality test specimens with absolute densities above 0.95 g/cm^3 can be produced and the results can be compared to previous work. To minimize scatter in the mechanical properties, all the specimens were manufactured using the same CO₂-laser powered EOS P730 sinter station. Furthermore, all specimens were built at the same location in the build platform to guarantee equal cooling conditions after the

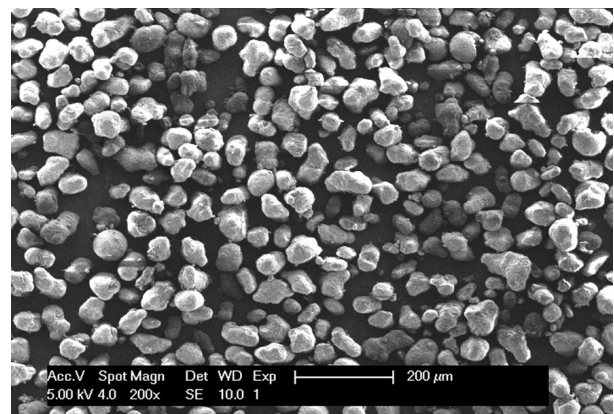


Fig. 2. SEM observation of PA12 powder particles.

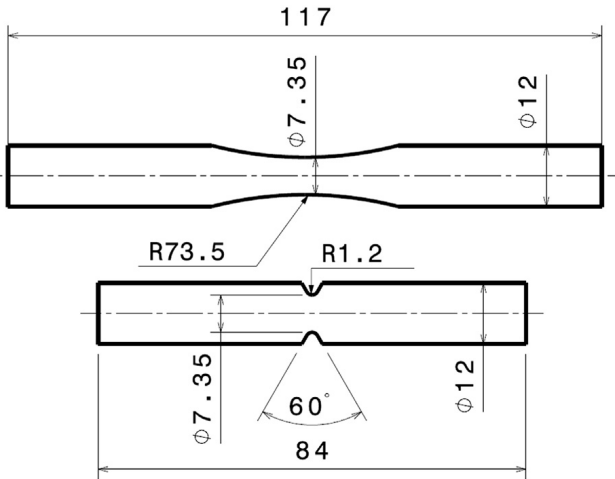


Fig. 3. Geometry of the notched and unnotched cylindrical test specimens in PA12.

laser sintering. No treatment was applied after laser sintering and so the as-built material behavior is studied.

2.3. Injection molding

The same starting material has to be used to be able to study the influence of the manufacturing technique (SLM and IM) on the mechanical fatigue properties. However, the powder particles that are used for laser sintering are too small to use as starting material for injection molding. To resolve this, cold isostatic pressing (CIP) was used to form long cylinders of compressed PA12 powder at 3000 bar, which were then cut into smaller granules. These granules were dried prior to injection molding using hot air to avoid deterioration of mechanical properties of the final products caused by moisture in the starting material.

To produce specimens with identical geometry as the SLS specimens, a new injection mold was designed as indicated in Fig. 5. The following measures were taken to improve the quality of the end-product.

- Notched and unnotched specimens are produced from one unique mold to minimize differences in surface quality. Since the cavity of the notched specimens (B) is

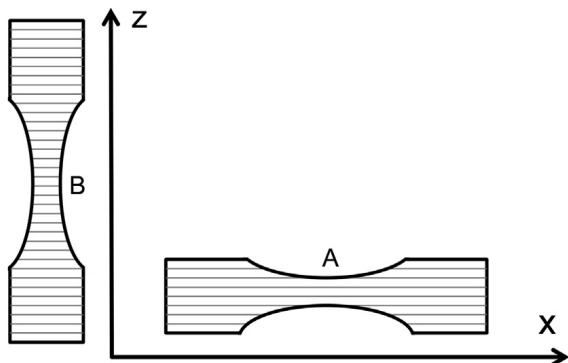


Fig. 4. Scan direction for the SLS specimens, SLS-x (A) and SLS-z (B).

Table 1

Process parameters for selective laser sintering of PA12 powder.

Laser beam diameter	0.65–0.7 mm
Particle diameter	60–90 μm
Powder bed temp.	170 °C
Frame temp.	140 °C
Layer thickness	0.12 mm
Energy density	0.031 J/mm ²
Cooling time	12 h

smaller than the cavity of the unnotched specimens (H), both cavities cannot be filled at the same time. Therefore, an adjustable insert (E) is used to route the plastic to one of the two cavities.

- To avoid weld lines in the critical section in the middle of the specimens, a side gate (C) is used such that the plastic first stops against the edge of the specimen and then gradually fills the cavity.
- Air vents (A) are located at the end of the cavities to release trapped air.
- The injection and ejection mold are equipped with preheating channels (G) to avoid large temperature gradients in the injected plastic.
- Moldflow was used to numerically simulate the injection molding process. Based on this simulation, the location of runners and gate was optimized and the process parameters were determined.

Finally, the specimens are produced using an Engel ES200/35 HL injection molding machine with process parameters as indicated in Table 2. No treatment was applied after the injection molding and so the as-molded material behavior is studied.

3. Experimental setup

3.1. Fatigue analysis

A closed loop servo-hydraulic test rig was used to apply a fluctuating tension/compression load to the specimens. No mean stress was applied ($R = -1$). For the temperature measurements, two devices were used: a thermocouple

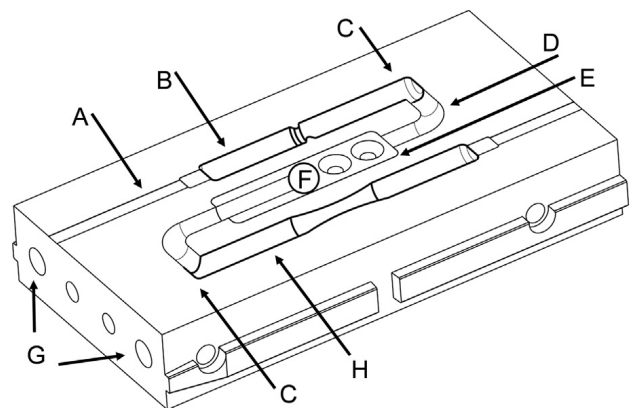


Fig. 5. Injection mold with air vents (A), cavity for notched geometry (B), gate (C), runner (D), adjustable insert (E), sprue (F), mold preheating channels (G), cavity for unnotched geometry (H).

Table 2
Process parameters for injection molding of PA12 granules.

Mould temperature	60 °C
Nose temperature	230 °C
Hopper temperature	40 °C
Injection pressure	50 bar
Injection speed	60 mm/s
Hold pressure	10 bar
Hold time	3 s
Cooling time	30 s

and an “EasIR-9” infrared camera. The thermocouple was attached to the critical area of the test specimen. The thermal camera was used to monitor the heat dissipation during testing.

The results of tensile tests were used to determine the first stress amplitude for fatigue testing at 60% of the UTS. At least 15 specimens were used for every Wöhler-curve. All tests were performed with fixed stress amplitude and a fixed test frequency of 3 Hz. No artificial cooling was applied. The fatigue tests were performed in a conditioned test lab with room temperature of 20.8 ± 0.3 °C and relative humidity of $50 \pm 5\%$. To obtain reproducible results, the specimens were stored for 48 h in the conditioned room before testing. Careful attention was given to a proper alignment of the test specimens in order to avoid secondary bending stresses.

3.2. Thermal analysis

Differential Scanning Calorimetry (DSC) tests were carried out using 6 ± 0.5 mg of material cut from the side and fracture surfaces of SLM and IM parts. The starting powder and the granulate for injection molding were subjected to a temperature scan from -30 °C to 300 °C and back with a heating and cooling rate of 10 °C/min.

3.3. Microstructural analysis

To analyze the microstructure and local density of IM- and SLS-parts, 10 mm long sections were cut from the specimens and mounted using a cold-setting resin. Wet grinding was then used with 240 to 1200-grit papers followed by automatic diamond polishing with $3 \mu\text{m}$ paste on a synthetic cloth. A Philips reflected light microscope was used to study the number and distribution of pores in these cross-sections. The crystal structure was also analyzed using a Siemens D500 X-ray diffractometer at room temperature with nickel filtered Cu-K α radiation of wavelength 0.154 nm and a reflection angle ranging from 4° to 55° .

4. Test specimen properties

Although the same raw material is used for the manufacturing of selective laser sintered and injection molded specimens, the material structure and the material quality is not the same. This leads to different failure mechanisms and different mechanical properties. To facilitate improved understanding of this difference in mechanical properties and fatigue behavior of SLS and IM

specimens, the specimen quality and material structure was studied as described below. Table 3 summarizes the most important results.

4.1. Dimensions

The actual dimensions of all the test samples were determined using a light microscope. The critical diameter and notch radius are most important since they determine the region where fatigue failure will occur. The measurements show a deviation from the desired values (Ref. in Table 3) which is taken into account when calculating the stress in the cross-sections. By doing so, the variation of the cross-sectional dimensions of SLSx, SLSz and IM specimens will not influence the results of the fatigue experiments. Specimens produced with the same manufacturing technique show minimal variation in dimensions.

4.2. Density

It is well known that the density of selective laser sintered and injection molded components has an important influence on the mechanical properties [15,16]. Regions in the material which are not fully dense have a lower mass/volume ratio leading to lower absolute strength and stiffness. Pores may also act as stress concentrators, leading to crack initiation and failure. Even with measures to avoid pores in the material, it is very difficult to produce parts with exactly the same density. During sintering, parts in the middle of the platform will experience a lower cooling rate than parts on the outside of the platform. This is one reason for the variation in quality that is inherent in the SLS process.

The global density of all the test specimens was determined using accurate measurements of the geometry and mass. The average results of these measurements for all the SLS-x, SLS-y and IM specimens are summarized in Table 3. Because of the optimized process parameters for both SLS and IM, all the samples have high global densities and there is only a small difference in global density between IM-parts and SLS-parts. The material density of the IM-parts is, however, not uniform over the longitudinal direction of the specimens. The size, number and distribution of pores in the test specimens were analyzed using optical light microscopy and digital image processing. Fig. 6 shows the results of these techniques applied to a cross-section of a SLSx part. First, the complete cross-section is put together by overlapping 8 separate images from the microscope.

Table 3
Properties of SLS and IM specimens in PA12.

Parameter	Unit	Ref.	SLSx	SLSz	IM
Critical diameter	mm	7.35	7.49 ± 0.11	7.41 ± 0.14	7.10 ± 0.05
Notch radius	mm	1.20	1.16 ± 0.22	1.07 ± 0.14	1.22 ± 0.17
Global density	g/cm^3	–	0.97 ± 0.01	0.98 ± 0.01	0.99 ± 0.01
Max. local density	g/cm^3	–	0.97	0.98	1.03
Ra-value	μm	–	15	18.5	0.7
Melting temp.	°C	–	179	179	186
Crystallinity	%	–	28	28	25
Crystal structure	–	–	$\alpha + \gamma$ form	$\alpha + \gamma$ form	γ form

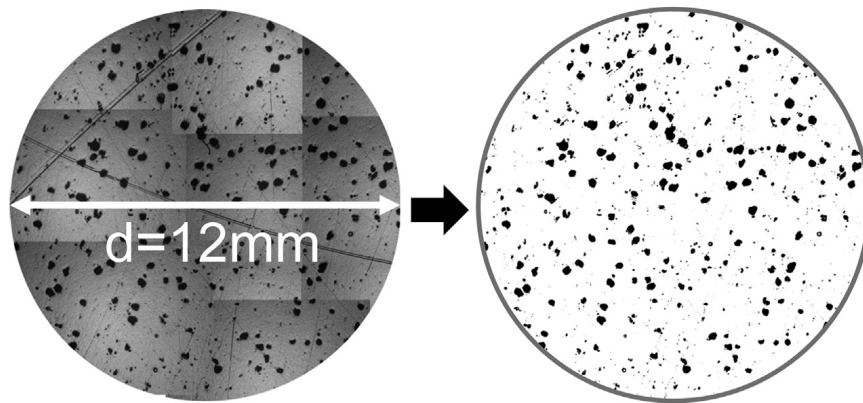


Fig. 6. Size and distribution of pores in the cross-section of a SLSx specimen.

Then, software is used to apply a Black/White threshold and to filter out the remaining scratches that occurred from grinding and polishing. In a final step, the percentage of black pixels is determined and the size and distribution of these black pores is studied.

For the SLSx and SLSz specimens, irregular pores with lengths ranging from 10 μm to 200 μm are found to be randomly spread over the cross-section. Furthermore, tests on different cross-sections indicate that pores in SLSx and SLSz parts have the same distribution and size over the whole length of the specimens. This is validated by determining the global density of a specimen based on calculations of the percentage of pores in one cross-section. In Fig. 6, there are 95.3% white pixels and the density of 100% dense PA12 equals 1.03 g/cm^3 . Assuming a uniform distribution of pores over the length of the specimen, the global density can then be calculated as 0.953×1.03 which equals 0.982 g/cm^3 . This is very close to the measured density of 0.98 g/cm^3 .

For the IM specimens, a non-uniform density distribution is observed. Near the end of the specimens, large pores of 800 μm diameter are found that are caused by a blocked air vent in the injection mold. The rest of the IM-parts, including the critical section for fatigue failure, are found to be fully dense (1.03 g/cm^3).

4.3. Surface roughness

The surface roughness was determined with a Taylor-Hobson Form Talysurf-120L apparatus. A measuring probe with radius of 2 μm was used to scan a straight track of 35 mm in the longitudinal direction at 0.5 mm/s. Special care was taken to limit the measurement force.

The surface roughness (R_a) measurements indicate a very smooth surface for the IM-parts, which is caused by the fine surface quality of the mold and the shrinkage of the material after injection. The surface of the SLM-parts is rougher because of the layer-wise production technique. After scanning the final contour of each layer, unmolten powder particles will stick to this contour leading to a porous outer material layer. Furthermore, the parts with scanning direction perpendicular to the loading direction (B in Fig. 3) have a slightly rougher surface than the parts

with scanning direction parallel to the loading direction (A in Fig. 3). In the first case (B), the roughness is measured over different layers while in the second case (A) the roughness is measured over the contour of one layer.

The difference in surface roughness between IM- and SLS-parts will have a negligible influence on the mechanical properties that are analyzed in this work because the specimens are loaded in tension/compression and previous research has shown that cracks initiate from pores or material imperfections in the specimens rather than from the surface [14]. This is in accordance with a recent study by Blattmeier et al. on the influence of surface characteristics on fatigue of SLS parts [17].

4.4. Microstructure

DSC was applied to study temperature transitions, melting range and degree of crystallinity of the SLS and IM specimens. Generally, all the DSC-curves follow the same shape showing three distinct features: (i) a small dent close to 50 $^{\circ}\text{C}$ indicating the glass transition temperature, (ii) a negative peak in the melting region between 177 $^{\circ}\text{C}$ and 186 $^{\circ}\text{C}$ and (iii) a positive peak close to 157 $^{\circ}\text{C}$ indicating the solidification region. Since all the examined specimens yield approximately the same DSC-curves, only one region of interest between 160 $^{\circ}\text{C}$ and 200 $^{\circ}\text{C}$ is plotted in Fig. 7, showing the average melting behavior of the powder and material taken from IM and SLS specimens.

The area of the melting peaks represents the heat of melting in J/g. The percentage of crystallinity ($C_{\%}$) of the semi-crystalline PA12 material can then be expressed as shown in Formula 1 [12], where the heat of melting for a 100% crystalline specimen of SLS-PA12 equals 209.3 J/g according to Gogolewski et al. [18].

$$C_{\%} = \frac{\text{Heat of melting (sample)}}{\text{Heat of melting (100\% crystalline specimen)}} \quad (1)$$

The powder and the granulate show exactly the same curve with melting temperature (T_m) of 186.23 $^{\circ}\text{C}$ and crystallinity (C) of 45%. This corresponds very well with the findings of Savalani, M.M ($T_m = 187.26$ $^{\circ}\text{C}$) [19]. Furthermore, this indicates that the production technique to

manufacture granulate from PA12 powder did not change the thermal properties of the PA12 material.

Analyzing fatigue loaded or original specimen material does not yield different values for the measured melting temperature or crystallinity. This means that fatigue testing does not have a permanent influence on the material's degree of crystallinity and thermal properties. However, during fatigue testing, the amorphous regions in the polymer will stretch and elongate and the specimen temperature will rise above the glass transition region. This can cause the crystal structure to change from γ -form to α -form, as described in the next section. After fatigue testing, the temperature will decrease and the original crystal structure reforms.

Fig. 7 indicates a distinct difference in melting temperature and crystallinity between powder, SLS and IM material. This difference is clearly caused by the thermal history of the material. The IM material was fully molten just before injection and then cooled rapidly after ejection. This rapid cooling allows less crystal growth, and hence relatively low crystallinity is observed. The SLS material was also fully molten during laser sintering but the cooling rate after processing is much lower, which allows the molecules enough thermal mobility to transform to a more crystalline structure.

Another interesting feature in the DSC-curves of some SLS samples is the small additional peak with minimum at 186 °C, which corresponds to the melting temperature of the PA12 powder. This additional peak was previously analyzed by Zarringhalam and Hopkinson, who found that the microstructure of an SLS part consists of fully molten particles and unmolten particle cores surrounded by spherulites [12]. These unmolten powder particles have the same melting temperature as the original powder, causing the additional small peak at 186 °C. The results of the DSC-experiments in this study are in correspondence with that theory. However, most of the DSC samples from SLS specimens indicate fully molten material. Furthermore, it is important to note that special care should be taken to use DSC samples that actually represent the cross section of the material. Samples taken from the surface will also indicate

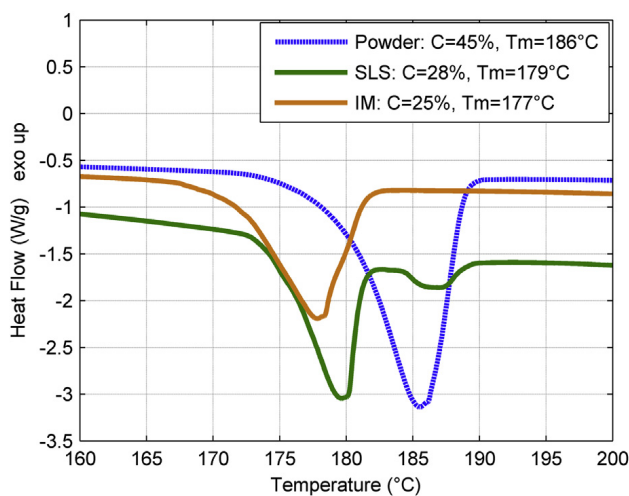


Fig. 7. DSC curves for IM, SLSx and SLSz material.

this small additional peak at T_m and increased crystallinity. This is, however, caused by the partially molten powder particles that are attached to the outer surface layer after final contour scanning, and that are not representative of the average properties of the specimen.

Once above the melting temperature, the 'memory effect' in the material is destroyed. The heat flow curves of all the specimens coincide and no temperature difference is seen on reaching the solidification temperature of 157 °C.

4.5. Crystal structure

The crystal structure of polyamides has been deeply studied and is known to be in the so-called α and γ -forms. The α -form consists of a monoclinic or triclinic lattice with chains in fully extended planar zigzag arrangement whereas the γ -form is a pseudo-hexagonal packing of 2₁ chains [6,20].

Atkins found that the α -form transforms to the γ -form when heated to T_m . This pseudo-hexagonal phase can then be 'frozen' by rapid cooling conditions [21]. If these crystals are heated above T_g , they revert to the monoclinic phase and, if temperature is increased further, the structure will start to transform again to the pseudo-hexagonal phase.

In this work, X-ray diffractions were taken from the PA12 powder and from notched and unnotched SLS and IM parts. The radiation was detected in the range of 4–50 degrees. Fig. 8 presents the results of these tests. It was found that the notched and unnotched specimens all show the same trend as well as the SLSx and SLSz parts. Furthermore, a small reflection peak was detected at 5.6 degrees for all the measurements. Distinct crystalline peaks are seen in the region between 20 and 24 degrees, which is shown more in detail in Fig. 9. The PA12 powder shows two reflection peaks, which is in accordance with similar experiments by Salmoria et al. [6] The first peak at 21.2° indicates the γ -crystalform (100) and the second peak at 22.2° indicates the α -crystalform (010/110) [6]. After laser

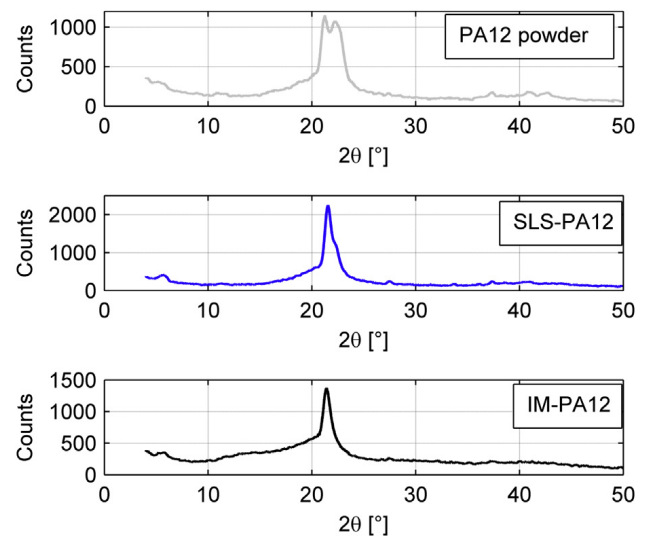


Fig. 8. X-ray diffractograms for PA12 powder, SLS-PA12 and IM-PA12.

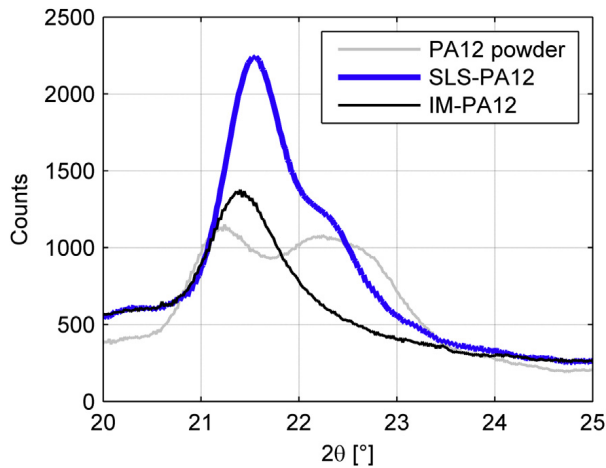


Fig. 9. Detail of X-ray diffractograms for $20^\circ < 2\theta > 25^\circ$.

sintering, the γ -form is more pronounced but the α -crystal form is still present. After injection molding, the rapid cooling conditions caused the material to crystallize exclusively in the γ -form.

In general, the XRD measurements indicate a small difference in crystal structure between SLS and IM parts caused by the slow cooling (12 h) of the SLS specimens compared to the rapid cooling (30 s) of the IM specimens. Furthermore, it is interesting to note that the crystal structure can change during fatigue testing. In the following section it is shown that the specimen temperature rises above the glass transition region. Consequently, the γ -form can transform to the α -form. This crystalline transition under increased temperature and uni-axial loading may cause a shift of the molecular chains in a preferential orientation, leading to improved fatigue resistance.

5. Mechanical properties

5.1. Tensile tests

To determine appropriate stress levels for the fluctuating load, tensile tests were performed on the unnotched specimens made by IM and SLS. The results of these tests are summarized in Table 4. The following phenomena are noted.

- There is only a small difference in ultimate tensile strength (UTS) between all the specimens.
- The difference in fracture strain and modulus of elasticity clearly shows that SLS parts are more brittle than IM parts. This is also visible by examining the fracture surfaces of the specimens. For the SLS-parts, the fracture surface is flat and perpendicular to the loading direction.

Table 4
Results of tensile tests on unnotched SLS and IM parts in PA12.

Parameter	Unit	SLSx	SLSz	IM
UTS	MPa	52	49	53
E-modulus	MPa	2080	2158	1701
ϵ -fracture	%	7	4	97

For the IM-parts, necking and strain hardening occurs leading to an irregular and elongated fracture surface.

- SLS-x and SLS-z parts show similar values for tensile strength and modulus of elasticity. The fracture strain however is much lower for the SLS-z parts. This indicates that for quasi static loading, interlayer fracture (between two successive layers) is more brittle than intralayer fracture (within the layers).

To analyze the notch-sensitivity, tensile tests were performed on the notched samples. It was found that the notched specimens reach higher UTS than the unnotched test specimens, as shown in Fig. 10 at 10^0 cycles. This effect is particularly shown in IM specimens, with an increase in UTS from 53 MPa to 62 MPa. This effect is attributed to notch strengthening, i.e. increasing load carrying capacity of the notched area after local yielding. Voids will nucleate in the localized plastic zone near the notch when the stress is increased further. This will eventually lead to crazing and macroscopic brittle failure perpendicular to the loading direction.

5.2. Fatigue tests

The results of the fatigue experiments are presented in Fig. 10 as seven SN-curves on a semi-logarithmic scale. The four Wöhler curves of the unnotched (UN) specimens can be found at the bottom of Fig. 10. Also, the fatigue results from a previous study by the authors (UN_Ref. in Fig. 10) are found in this region [14]. The variation between these lines is limited, indicating the similar fatigue life of the SLSx, SLSz and IM specimens at given stress amplitude. This shows that the SLS parts have equal intra- and interlayer fatigue strength, and that the small differences in crystal structure, crystallinity, surface roughness and density between SLS and IM parts does not affect the fatigue failure of the unnotched samples. The SN-lines also converge to a clear endurance limit around 18 MPa.

It is remarkable that the pores in the unnotched SLS parts, as shown in Fig. 6, do not have a more pronounced negative impact on the fatigue life. When loaded, the porous material will deform and microvoid coalescence occurs. However, this does not lead to rapid crack initiation and crack propagation as expected. The fracture mechanism is somehow delayed. Because of the high molecular mobility, resulting from the high local cyclic stresses near the pores or initial cracks, the inner material temperature increases. This temperature effect leads to three possible phenomena delaying fatigue failure initiated from pores in the material.

- A local melt zone is formed, leading to stabilization of crack growth.
- Above the glass transition temperature, relative sliding between chain molecules occurs. Amorphous polymer chains are stretched and elongated, allowing more elasticity.
- The increased temperature alters a transformation of the crystal structure from the γ -form to the α -form. This can cause a shift of the molecular chains in a preferential orientation leading to improved fatigue resistance.

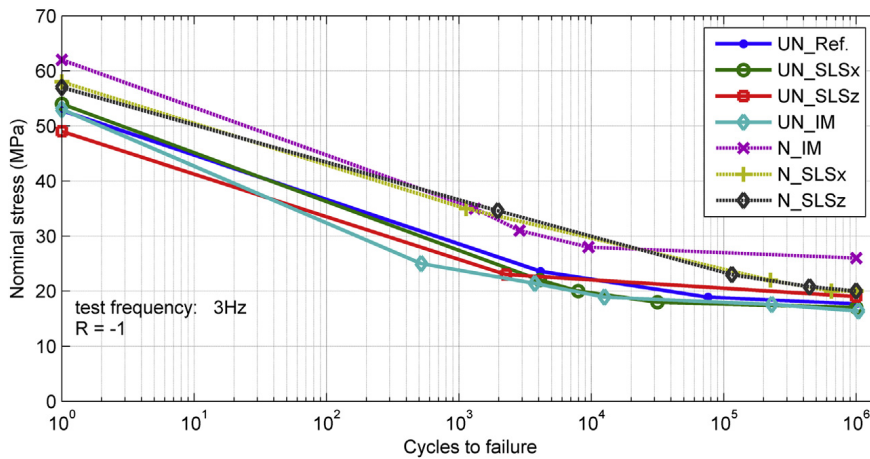


Fig. 10. SN fatigue curves for notched (N) and unnotched (UN) SLS and IM specimens.

Eventually, cracks will grow and extensive yielding occurs, leading to ductile fatigue failure. In general, the fatigue tests resulted in ductile fracture surfaces with semi-spherical depressions for the unnotched specimens and brittle fracture surfaces for the notched specimens. This indicates the reduced ductility near the notch caused by the presence of a complex triaxial stress field and steep stress gradient. The three Wöhler curves for the notched (N) specimens are shown at the top of Fig. 10, indicating improved fatigue resistance compared to the unnotched specimens. This is attributed to the notch strengthening that was also observed during tensile testing.

5.3. Hysteresis

It is clear that fatigue failure is caused by a combination of mechanical and thermal loading. Since no artificial cooling was applied and a fixed test frequency of 3 Hz was used, the temperature rise in the material plays an important role in the fatigue life of all the test specimens. During fatigue testing, the surface temperature was measured with a thermocouple. For the notched specimens, an infrared camera was used to measure the temperature in the root of the notch during fatigue loading. No noticeable difference was detected in temperature behavior of SLS and IM specimens. Fig. 11 shows the increase in maximum surface temperature for a notched specimen measured with the IR-camera as a function of time. Initially, a linear increase in surface temperature is seen, as indicated by the trend line in Fig. 11. Starting from 34 °C, there was rapid growth in temperature followed by final failure. After failure, a temperature of 130 °C was recorded which is the average inner material temperature measured on the fracture surface. Measurements on unnotched specimens show a very similar temperature-time history. When the local stress amplitude is lower than the endurance limit, quasi-isothermal conditions occur and the specimens endure at least 10⁶ load cycles.

A convenient way to analyze the thermo-mechanical behavior of the fatigue loaded nylon specimens is to plot the stress as a function of strain for each load cycle. Fig. 12 shows three of these typical hysteresis loops taken from a

notched IM specimen. For the sake of clarity, only the first, middle and final load cycle were plotted.

If the temperature of the semi-crystalline PA12 reaches the glass transition region (23.5–55°), the amorphous polymer chains will soften [14]. As a result, these chains will reorient themselves (crystallization) and by doing so the stiffness will decrease, leading to larger deformations at the same stress level. This is clearly visible on the decreased slope of the hysteresis loop measured just before fatigue failure. Furthermore, the origins of these curves have shifted to the right, indicating that there is a continuous increase of strain in time when loading at constant stress amplitude. This behavior is called cyclic creep or ratcheting.

The area within these hysteresis loops equals the energy loss during a given load cycle. For the notched specimens, this energy loss is small during the first load cycles and the hysteresis loop is almost a straight line. In the middle of the fatigue life of the specimens, a small amount of energy loss is seen. When the temperature exceeds the glass transition region, the molecular mobility grows, causing more dissipated energy in the form of heat, as indicated by the area within the final hysteresis loop.

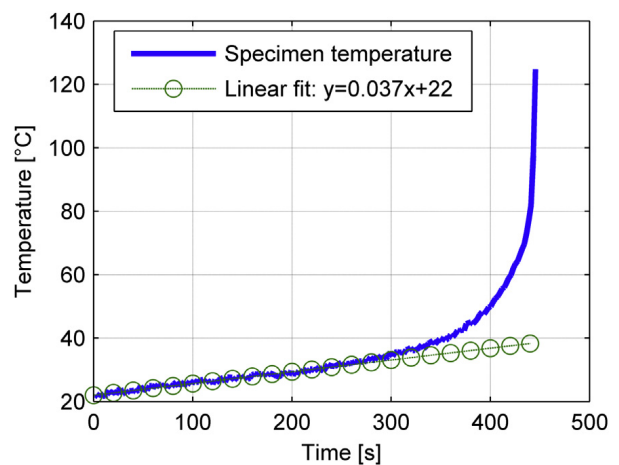


Fig. 11. Temperature accumulation of the outer material surface during fatigue testing of a notched injection molded specimen.

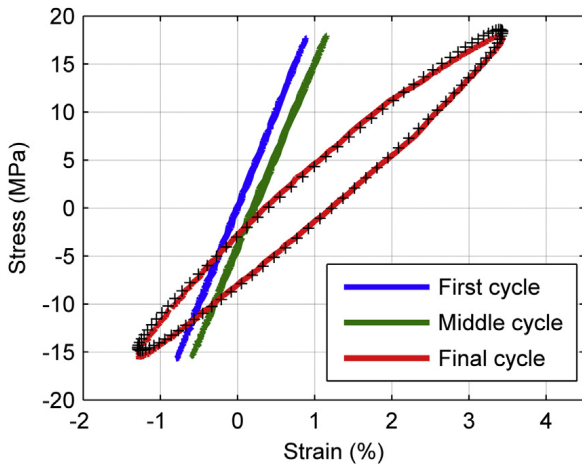


Fig. 12. Hysteresis loops for a notched injection molded specimen during the first, middle and final load cycle.

The total energy loss per unit of volume during one fatigue cycle can be calculated using the stress amplitude (σ_a), the strain amplitude (ϵ_a) and the phase difference (δ) between stress and strain, as indicated in Formula 2. By multiplying by the test frequency (f), the total power loss per unit of volume and per fatigue cycle is determined, as shown in Formula 3. This power loss is expressed in W/m^3 and can be partitioned into heat transfer (P_{HT}), sample heating (P_S) and sample fracture (P_F), as indicated in Formula 4.

$$\Delta D = \pi \times \sigma_a \times \epsilon_a \times \sin \delta \quad (2)$$

$$\dot{\Delta} D = f \times \pi \times \sigma_a \times \epsilon_a \times \sin \delta \quad (3)$$

$$\dot{\Delta} D = P_{HT} + P_S + P_F \quad (4)$$

The heat transfer can then be partitioned into conduction (P_k), convection (P_h) and radiation (P_z), as shown in Formulas 5–8. The heat transfer coefficients k , h and z for conduction, convection and radiation were determined using Dubbel's work to be $0.25 W/mK$, $7.28 W/m^2 K$, and $5.67 E^{-8} W/m^2 K^4$, respectively [22]. All the required temperatures were determined using the thermocouple and IR-camera during fatigue testing.

$$P_{HT} = P_k + P_h + P_z \quad (5)$$

$$P_k = \frac{k \cdot A}{V} \times \frac{dT}{dx} \quad (6)$$

$$P_h = \frac{h \cdot A}{V} \times (T_0 - T_\infty) \quad (7)$$

$$P_z = \frac{z \cdot A}{V} \times (T_0^4 - T_2^4) \quad (8)$$

The power to heat the specimen is determined using Formula 9 with an average density (ρ) of $1030 kg/m^3$ and specific heat capacity (C_p) of $1700 J/kgK$ [22]. The required temperature-time data was taken from the IR-camera measurements.

$$P_s = \rho \times C_p \times \frac{\Delta T}{\Delta t} \quad (9)$$

By determining the total power dissipation from the hysteresis loops and after solving Equations 5–9 for power dissipated by heat transfer, the unknown power needed for crack growth (P_F) can be calculated using Formula 4. For the notched IM specimen with temperature-time data shown in Fig. 11, and three hysteresis loops shown in Fig. 12, the total dissipated power equals $0.22 W/cm^3$, $0.28 W/cm^3$ and $1.5 W/cm^3$, respectively. During the first load cycles, all the dissipated power is transformed into heat (P_{HT} and P_S). In the middle of the fatigue life of the specimens, 5.6% of the total dissipated power is used for fracturing the specimen (P_F). During the final load cycle, P_F equals 8% of the total dissipated power. Calculations for other specimens indicate the same trend which indicates that the PA12 specimens can clearly absorb a substantial amount of energy without fracturing. Further work is needed to determine the heat transfer coefficients with higher accuracy so that P_F can be used to validate fracture theories.

6. Conclusions

A study was made of the fatigue properties of as-built nylon parts produced by selective laser sintering (SLS) and injection molding (IM). Both notched and unnotched specimens were produced starting from one unique batch of semi-crystalline polyamide 12. The material quality of these specimens was carefully examined and found to be acceptable for the use in various functional applications. To study and understand the acting failure mechanisms, the thermal properties, microstructure and hysteresis behavior was analyzed. The most important conclusions of this work are summarized below.

- The fatigue failure of all the specimens is controlled by cyclic mechanical loading in combination with temperature effects.
- The building direction of the selective laser sintered parts has negligible influence on the fatigue properties, the density, the degree of crystallinity and the crystal structure of the samples examined in this study. This indicates that quasi-full powder melting occurred leading to equal inter- and intra-layer fatigue strength.
- Despite the observed difference in failure strength, material density, crystallinity and surface roughness, the injection molded and selective laser sintered samples have similar fatigue properties. Furthermore, all the SN-curves converge to a clear endurance limit $>18 MPa$. This indicates acceptable fatigue resistance for the notched and unnotched selective laser sintered components in PA12 given the applied test conditions and without the use of artificial cooling.
- Future work is needed to study the impact of the test specimen geometry and temperature/frequency effects

on the failure mechanisms and fatigue properties of both notched and unnotched components.

Acknowledgements

This research is funded by a Ph.D grant of the Institute for the Promotion of Innovation through Science and Technology in Flanders (IWT-Vlaanderen). The authors would also like to acknowledge Toon Roels from Materialise for valuable discussions on material properties and the production of SLS-PA12 test specimens.

References

- [1] L. Lü, J. Fuh, *Laser-induced Materials and Processes for Rapid Prototyping*, Kluwer, London, 2001.
- [2] R. Noorani, *Rapid Prototyping: Principles and Applications*, Wiley, 2005.
- [3] R.D. Goodridge, C.J. Tuck, R.J.M. Hague, Laser sintering of polyamides and other polymers, *Prog. Mater. Sci.* 57 (2) (2012) 229.
- [4] G.V. Salmoria, J.L. Leite, Selective laser sintering of PA12/HDPE blends: effect of components on elastic/plastic behavior, *Polym. Test.* 27 (2008) 654.
- [5] M. Campbell, Performance of CF/PA12 composite femoral stems, *J. Mater. Sci. Mater. Med.* 19 (2008) 683.
- [6] G.V. Salmoria, J.L. Leite, R.A. Paggi, The microstructural characterization of PA6/PA12 blend specimens fabricated by selective laser sintering, *Polym. Test.* 28 (7) (2009) 1.
- [7] G.V. Salmoria, J.L. Leite, R.A. Paggi, Selective laser sintering of PA12/HDPE blends: effect of components on elastic/plastic behavior, *Polym. Test.* 27 (2008) 654.
- [8] G.V. Salmoria, J.L. Leite, Rapid manufacturing of PA/HDPE blend specimens by selective laser sintering: microstructural characterization, *Polym. Test.* 26 (2007) 361.
- [9] P. Marcelis, *Control of Selective Laser Sintering and Selective Laser Melting Processes*. PhD Thesis, KU Leuven, Belgium, 2007.
- [10] P. K. Jain, P.M. Pandey, P.V.M. Rao, Effect of delay time on part strength in selective laser sintering, *Int. J. Adv. Manuf. Technol.* 43 (2009) 117.
- [11] A. Becker, J.R. Grez, Elastic tensor stiffness coefficients for SLS Nylon 12 under different degrees of densification as measured by ultrasonic technique, *Rapid Prototyping J.* 14 (5) (2008) 260.
- [12] H. Zarringhalam, N. Hopkinson, Effects of processing on microstructure and properties of SLS Nylon 12, *Mater. Sci. Eng. A* 435 (2006) 172.
- [13] B. Caulfield, P.E. McHugh, S. Lohfeld, Dependence of mechanical properties of polyamide components on build parameters in the SLS process, *J. Mater. Process. Tech.* 182 (2007) 477.
- [14] B. Van Hooreweder, Microstructural characterization of SLS-PA12 specimens under dynamic tension/compression excitation, *Polym. Test.* 29 (2010) 319.
- [15] B. Van Hooreweder, Design and simulation of a novel multi-axial fatigue test rig, *Exp. Mech.* 52 (2012) 513.
- [16] J.P. Kruth, in: *Proceedings of the 3rd International Conference on Polymers and Moulds Innovations*, Gent, 2008, pp. 15–30.
- [17] M. Blattmeier, G. Witt, J. Wortberg, J. Eggert, J. Toepker, Influence of surface characteristics on fatigue behavior of laser sintered plastics, *Rapid Prototyping J.* 18 (2) (2012) 161.
- [18] S. Gogolewski, K. Czerniawska, M. Gasiorek, Effect of annealing on thermal properties and crystalline structure of polyamides, *Prog. Colloid Polym. Sci.* 258 (1980) 1130.
- [19] M.M. Savalani, *Selective Laser Sintering of Hydroxyapatite-polyamide Composites*. PhD Thesis, Loughborough University, Leeds, UK, 2006.
- [20] C.E. Fernandez, Compared structure and morphology of nylon-12 and 10-polyetherane lamellar crystals, *Polymer* 52 (2011) 1515.
- [21] E.D.T. Atkins, Structural and morphological investigations of nylon 8 chain-folded, lamellar crystals, *Polymer* 36 (1) (1995) 35.
- [22] H. Dubbel, W. Beitz, B.J. Davies, *Handbook of Mechanical Engineering*, Springer, London, 1994.